EVALUATION OF TURBULENCE MODELS TO PREDICT THE EDGE SEPARATION BUBBLE OVER A THIN AEROFOIL

A. L. T. Rezende, arezende@ime.eb.br
Department of Mechanical and Materials Engineering, IME - Military Engineering Institute, 22290-270, Rio de Janeiro, RJ, Brazil
A. O. Nieckele, nieckele@puc-rio.br
Department of Mechanical Engineering, PUC/Rio, 22453-900, Rio de Janeiro, RJ, Brazil

Abstract. *The flow field around a thin flat plate with a leading edge and an infinite wingspan at small incidences is a very complex flow due to the existence of laminar-to-turbulent transition, boundary layer separation, leading edge bubble and reattachment. Due to the flow complexity, its numerical prediction represents a considerable challenge. Therefore, the purpose of this study is the evaluation of turbulence models to predict this flow The solutions are obtained through the Reynolds Averaged Navier-Stokes (RANS) equations for the two-dimensional steady state flow, using the SST κ–ω 2-equations model and the more complex Reynolds Stress Tensor Model (RSM). The SST κ–ω assumes isotropic modeling of the Reynolds tensor and fails to reproduce some important features of this particular flow. To account for the anisotropy, the Reynolds Stress Tensor Model (RSM) solves an additional set of transport equations for the Reynolds stress tensor, which provides better results for both first and second order statistics, but introduces an anomalous flow pattern in the reattachment region, demands an increase in computational cost and produces convergence difficulties. Due to these difficulties, this work also presents the solution obtained with Large Eddy Simulation (LES) for the three-dimensional unsteady state flow, which provided considerable improvements in the results. Simulations were accomplished for 1 degree inclination angle of the flat plate with a Reynolds number of 2.13×10^5. The results are compared with available wind tunnel experimental data.*

Keywords*: flat plate, shallow incidence, RANS, LES, reattachment*.

1. INTRODUCTION

The objective of the present work is to analyze the incompressible turbulent flow around a thin flat plate with a leading edge and an infinite wingspan at small incidences. The simulations were accomplished with models based in the Reynolds Average Navier-Stokes equations (RANS) and Large Eddy Simulations (LES), with high Reynolds number. The performance of the turbulence models is evaluated by comparing with Crompton's experimental data (Crompton, 2001), which provides information regarding the flow around the thin flat plate, with incidence angles α varying from 1^o to 5^o and Reynolds number $Re = 2.13 \times 10^5$. This type of problem poses a challenge to the ability of the turbulence models to predict the flow, due to the presence of several flow structures. Therefore, a few works can be found in the literature, employing the same flow conditions and geometry as Crompton (2001) like Collie et al. (2008), Sampaio et al. (2006) and Rezende & Nieckele (2007) and Rezende et al. (2008).

Collie et al. (2008) investigated the flow considering incidence angles α equal to 1^o and 3^o, with the following two equation turbulence RANS models: $\kappa - \omega$ (Wilcox,1998) and SST κ–ω (Menter, 1994). A two dimensional domain was considered and it was concluded that the SST κ–ω model provided the best results.

Rezende and Nieckele (2007) analyzed the flow for inclination angles α equal to 1^o, 3^o and 5^o. The flow was also considered as 2D, but a finer mesh was employed with the one-equation Spalart-Allmaras model (Spalart & Allmaras, 1992) and SST κ–ω model (Menter, 1994). The Spalart-Allmaras model demonstrated certain deficiency in its predictions, in spite of being projected for aerodynamic applications. The results obtained with the SST κ–ω model were superior to Collie et al. (2008) results, due to the mesh refinement.

The Reynolds Stress Model - RSM (Launder, 1989) and the v^2f model (Durbin,1995) were employed by Rezende et al. (2008) to capture the turbulence anisotropy, for $\alpha = 1^o$. Better predictions were obtained with the RSM model only for the second order statistics, while poor results were predicted with the v^2f model, especially for high Reynolds numbers.

Sampaio et al. (2006) examined the problem with a 3D transient formulation through the Large Eddy Simulations (LES), with the traditional one-equation model (Kim and Menon, 1997) and with an alternative subgrid approach, named f-LES (Sampaio, 2006). Due to computational restrictions, Sampaio et al. (2006) investigated the inclination angle $\alpha = 1^o$ in a reduced domain and relatively coarse mesh. Although better results were obtained in relation to the RANS models predictions, it was concluded that a more refined mesh was needed.

Based on the results and conclusions of the previous papers, this work presents the numerical results for $\alpha = 1^o$ using three different methodologies: SST κ–ω model, RSM model and LES. The mesh was significantly refined mesh, in order to guarantee $y^+ \approx 1$ at the first grid point near the plate. The SST κ–ω model was selected because it presented the best result with the RANS methodology in previous investigations, while the second order RSM model was selected since it is capable of predicting flow anisotropy. Finally, the LES model with the Dynamic Smagorinsk sub-grid model (Germano et al., 1991; Lilly, 1992) was investigated, once Sampaio et al. (2006) have declared the need of refined mesh.

2. FLOW OVER A THIN FLAT PLATE

Understanding the flow around the thin flat plate at shallow incidence can help in the design of airfoils and sails as well as flexible wing-based micro air vehicles. The flow around an inclined flat plate with a sharp leading edge, as shown in Fig. 1, induces a long and thin bubble, denominated "thin aerofoil bubble". At zero incidence angle, the stream is laminar and attached on both sides, generating zero lift (assuming equal surface profiles). If the plate has an incidence angle, the stagnation point moves to the inferior surface. The boundary layer around the leading edge is very thin, and it is expected to separate immediately, due to the flow direction change. As shown in Fig. 1, there is a dividing streamline which separates the bubble from the outer flow and which rejoins the surface at the reattachment point. If the incidence angle is sufficiently small (usually smaller than 7 degrees), the flow reattaches at the upper surface at a point which moves gradually downstream with increasing incidence angle. For greater angles, there is no reattachment point, and the bubble enlarges downstream into the wake (Newman and Tse, 1992). Due to the fixed separation point the flow is insensitive to a change in Reynolds number, and transition will occur soon after separation (Crompton, 2001).

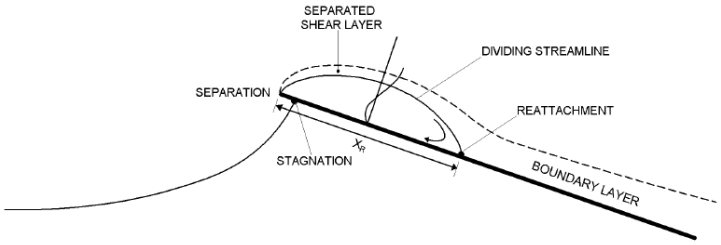

Figure 1. Simplified model of a thin aerofoil separation bubble.

Subsequent to separation, the shear layer suffers transition very close to the leading edge. The turbulent shear layer increases quickly and has a high entrainment rate; it then reattaches further downstream and bifurcates. Part of the flow is directed to upstream to feed the shear layer. The resultant backflow reduces the pressure at the surface and helps to bend the shear layer back to the reattachment point. The remaining flow is driven downstream where reverts gradually to an attached turbulent boundary layer before reaching the trailing edge (assuming there is enough length left after reattachment).

This complex flow around a plate at the shallow incidence has been experimentally investigated by Crompton (2001). Detailed velocity and turbulence statistics were measured in wind tunnel for the leading edge bubble with the use of Laser Doppler Anemometry (LDV) for inclination angles of the flat plate varying from 1 to 5 degrees with a Reynolds number based on the chord c equal to 2.13×10^5.

3. MATHEMATICAL MODEL

The equations that describe the incompressible fluid movement are the continuity and momentum equations, respectively

$$\frac{\partial u_j}{\partial x_j} = 0 \quad ; \quad \left(\frac{\partial u_i}{\partial t} + \frac{\partial u_i u_j}{\partial x_j} \right) = g_i - \frac{1}{\rho}\frac{\partial p}{\partial x_i} + \frac{\partial}{\partial x_j}\left(\upsilon \frac{\partial u_i}{\partial x_j} \right) \tag{1}$$

where u_i is velocity vector**,** ρ is the density, $\upsilon = \mu/\rho$ is the cinematic viscosity, μ is the molecular viscosity, p is the pressure and g_i is the acceleration of gravity.

The Reynolds-averaged approach is based on decomposing the velocity as $u_i = \overline{u}_i + u_i'$ where $\overline{u}_i$ is the average velocity vector and u_i' the velocity vector fluctuation. The average continuity and momentum equation (RANS), for a steady state incompressible flow is given by

$$\frac{\partial \overline{u}_j}{\partial x_j} = 0 \quad ; \quad \left(\frac{\partial \overline{u}_i}{\partial t} + \frac{\partial \overline{u}_i \overline{u}_j}{\partial x_j} \right) = g_i - \frac{1}{\rho}\frac{\partial \overline{p}}{\partial x_i} + \frac{\partial}{\partial x_j}\left(\upsilon \frac{\partial \overline{u}_i}{\partial x_j} - \overline{u_i' u_j'} \right) \tag{2}$$

Equation (2) has the same form of the Navier-Stokes equation, but now it has an additional term, the turbulent Reynolds stress term, $-\overline{u_i' u_j'}$, representing the influence of the fluctuation on the average flow. In order to close Eq. (2), the turbulent Reynolds stress must be determined. It can be directly modeled through the solution of its conservation equation, with corresponds to the Reynolds Stress Models (RSM), or it can be modeled by employing the Boussinesq hypothesis, based on the turbulent viscosity concept. With the Boussinesq hypothesis, the turbulent stress is obtained through an analogy with Stokes law, i.e., the stress is proportional to the mean deformation rate,

$$\overline{u_i' u_j'} = -2\,\overline{S_{ij}}\,\upsilon_t + \frac{2}{3}\kappa\,\delta_{ij} \quad ; \quad \overline{S_{ij}} = \frac{1}{2}\left(\frac{\partial \overline{u_i}}{\partial x_j} + \frac{\partial \overline{u_j}}{\partial x_i}\right) \quad ; \quad \kappa = \frac{1}{2}\overline{u_i' u_i'} \tag{3}$$

where $\overline{S_{ij}}$ is the average deformation rate, κ is the turbulent kinetic energy and $\upsilon_t = \mu_t / \rho$, where μ_t is the turbulence viscosity, which is defined in accordance with the models.

In the Large Eddy Simulation (LES) approach the governing equations are derived through the application of a spatial operator filter in the continuity and momentum equations, Eq. (1). The spatially-filtered Navier Stokes for an incompressible now can be written as:

$$\left(\frac{\partial \overline{\overline{u_j}}}{\partial x_j}\right) = 0 \quad ; \quad \left(\frac{\partial \overline{\overline{u_i}}}{\partial t} + \frac{\partial \overline{\overline{u_i}}\,\overline{\overline{u_j}}}{\partial x_j}\right) = g_i - \frac{1}{\rho}\frac{\partial \overline{\overline{p}}}{\partial x_i} + \frac{\partial}{\partial x_j}\left(\upsilon\frac{\partial \overline{\overline{u_i}}}{\partial x_j} - \tau_{ij}\right) \tag{4}$$

where $\overline{\overline{u_i}}$ and $\overline{\overline{p}}$ are the filtered velocity and pressure and τ_{ij} is the sub-grid tensor. The subgrid tensor is the result of commuting the filtering with the outer product and is defined as $\tau_{ij} = \overline{\overline{u_i u_j}} - \overline{\overline{u_i}}\,\overline{\overline{u_j}}$. A closed expression cannot be found for this subgrid tensor, and hence it must be separately modeled. In this investigation, τ_{ij} is modeled based on the Boussinesq hypothesis

$$\tau_{ij} = -2\,\overline{\overline{S_{ij}}}\,\upsilon_{SM} + \frac{2}{3}\left(\overline{\overline{u_k'' u_k''}}\right)\delta_{ij} \quad ; \quad \overline{\overline{S_{ij}}} = \frac{1}{2}\left(\frac{\partial \overline{\overline{u_i}}}{\partial x_j} + \frac{\partial \overline{\overline{u_j}}}{\partial x_i}\right) \tag{5}$$

where υ_{SM} is the turbulent subgrid viscosity, which was modeled with the Dynamic Smagorinsk subgrid model (Germano et al., 1991; Lilly, 1992), and $\overline{\overline{S_{ij}}}$ is the filtered deformation rate.

3.1. SST *k-ω* Model

The Shear-Stress Transport (SST) κ–ω RANS model (Menter, 1994) was proposed for aeronautical flows simulations with strong adverse pressure gradients and separation by combining the κ–ε and κ–ω models. For boundary layers flows, the κ–ω model is superior to the κ–ε model in the solution of the viscous near-wall region, and has been applied with success in problems involving adverse pressure gradients. However, the κ–ω model requires a non-zero boundary condition on ω for non-turbulent free-stream, and the calculated flow is very sensitive to the specified value (Menter, 1994). It has also been shown (Cazalbou *et al* , 1993) that the κ-ε model does not suffer this deficiency. Therefore, the SST κ–ω model blends the robust and precise formulation of the κ–ω model close to walls with the free-stream independence of the κ–ε model outside the boundary layer. To accomplish this, the κ–ε model is written in terms of the specific dissipation rate, ω. Then, the standard κ–ω model and the transformed κ–ε model are both multiplied by a blending function and both models are added together. This blending function F_1 is zero (leading to the standard κ–ω model) at the inner edge of a turbulent boundary layer and set to a unit value (corresponding to the standard κ–ε model) at the outer edge of the layer.

The turbulent eddy viscosity is formulated as follows:

$$\upsilon_t = \frac{\kappa/\omega}{\mathbf{max}\left(1\,;\, S F_2/(0.31\,\omega)\right)} \quad ; \quad F_2 = \tanh\left(\Phi^2\right) \quad ; \quad \Phi = \max\left(\frac{2\sqrt{\kappa}}{0.09\,\omega\,d}\,;\frac{500\,\upsilon}{d^2\omega}\right) \tag{6}$$

where $S = (\,2\,\overline{S_{ij}}\;\overline{S_{ij}}\,)^{0.5}$ is the modulus of the mean rate-of-strain tensor $\overline{S_{ij}}$, and F_2 is the blending function for the turbulent eddy viscosity in the SST κ–ω model, d is the distance to the wall. The turbulent kinetic energy κ and specific dissipation rate ω of the SST κ–ω model (Menter, 1994) can be determined by the solution of its conservation equations, where the set of closure constants for the SST κ–ω model ϕ are calculated using a blend between the constants ϕ_1 of the standard κ–ω and and ϕ_2 of the κ–ε model as $\phi = F_1\,\phi_1 + (1 - F_1)\,\phi_2$.

3.2. The Reynolds Stress Model (RSM)

The turbulence models based in the Boussinesq hypothesis represent a consolidated solution for the turbulence closure problem in the RANS models. However, in spite of recognized success in the solution of several turbulent

flows, such models present some deficiencies, usually associated to the limitations imposed by the concept of turbulent viscosity. The flows with strong turbulence anisotropy behavior are typical examples in which the Boussinesq hypothesis fails. An alternative for the closure problem consists in the direct solution of the transport equations for Reynolds Stresses (Reynolds Stress Model - RSM). Such closure models are called second order models (Launder, 1989). The Reynolds stress transport equation can be derived from the Navier-Stokes equation, being equal to

$$\frac{\partial \overline{u_i' u_j'}}{\partial t} + \frac{\partial \overline{u_i' u_j'}\,\overline{u_\ell}}{\partial x_\ell} = \frac{\partial}{\partial x_\ell}\left[\left(\mu + \frac{\mu_t}{\sigma_k}\right)\frac{\partial \overline{u_i' u_j'}}{\partial x_\ell}\right] + \left(-\overline{u_i' u_k'}\frac{\partial \overline{u_j}}{\partial x_k} - \overline{u_j' u'}_k \frac{\partial \overline{u_i}}{\partial x_k}\right) + \Phi_{ij} - \varepsilon\,\delta_{ij} \tag{7}$$

The first term of the right side is the diffusion rate (Lien and Leschziner, 1994) and the second is the production term (Launder, 1989). The term ε is the viscous dissipation calculated through its transport equation (Hanjalic, 1994), as in the $\kappa-\varepsilon$ model, σ_κ=1 is an empirical constant.

The pressure term Φ_{ij} involves correlations between pressure fluctuations and deformation rates. This term is not present in the turbulent kinetic energy equation, therefore it does not contribute to the total energy balance. It only acts to redistribute the energy among the normal components of the Reynolds stress (when $i= j$) and to reduce the shear stress (when $i \neq j$). Thus this term tends to turn the turbulence more isotropic. Modeling the Φ_{ij} term has been object of several works, representing a central theme in the development of those second order closure models. In the present study, the pressure term is modeled through the LRR modified model (Launder, Reece & Rody, 1975; Gibson and Launder, 1978), which includes an additional term for the redistribution of normal stress close the wall. This extra term damps the normal stress to the wall, while increases the shear stress parallel to the wall.

The RSM model was initially developed for turbulent flows without the influence of the wall, therefore it is necessary to define a specific treatment for this model at the near wall region area, especially because the present mesh was defined very fine, such that near the wall $y^+ \approx 1$, where $y^+ = \rho\, d\, u^* / \mu$, with $u^* = (\tau_w/\rho)^{0.5}$ as the friction velocity, d as the distance from the wall and τ_w as the wall shear stress. In accordance with Chen and Patel (1988), to simulate the flow behavior close the wall ($y^+ \approx 1$) with the RSM model, the whole domain must be subdivided in two areas. The first area is located close to the wall and is affected by the fluid viscosity. The other area, denominated totally turbulent, is located far from the wall. The definition of the two areas is determined through the wall Reynolds number $Re_w = \rho\, d\, \kappa^{0.5} / \mu$. In the totally turbulent region ($Re_w > 200$), the flow is solved by the RSM model as described. In the region close the wall ($Re_w \leq 200$) the Wolfshtein model (Wolfshtein, 1969) is applied.

3.3. Large Eddy Simulation - Dynamic Smagorinsk Model

The Dynamic Smagorinsk subgrid viscosity model selected to be investigated in the present paper is based on the Smagorinsly-Lilly Model (Germano et al., 1991; Lilly, 1992), where the sub-grid eddy-viscosity is

$$\upsilon_{SM} = (L_s)^2 \sqrt{2\overline{\overline{S_{ij}}}\,\overline{\overline{S_{ij}}}} \quad ; \qquad L_s = \mathbf{min}\left(k_v\, d, C_s \forall^{1/3}\right) \tag{8}$$

where $\overline{\overline{S_{ij}}}$ is the filtered deformation rate(Eq. 5), L_s is the mixing length for subgrid scales, and k_v is the von Kármán constant, d is the distance to the closest wall, C_s is the Smagorinsky constant and $\forall$ is the volume of the computational cell. In the dynamic approach, the Smagorinsky constant C_s is dynamically computed based on the information provided by the resolved scales of motion. Although, C_s can vary in time and space, to avoid instability it was clipped at zero and 0.23.

4. RESULTS

The thin flat plate investigated experimentally by Crompton (2001) was modeled with the geometry described in Fig. 2. The plate has a chord length c equal to 160 mm and a span of 800 mm giving an aspect ratio of 5, which is sufficient to supply nominally two-dimensional flow.

The wind tunnel investigation was carried at $Re = 2.13 \times 10^5$, where Re is defined as $Re = U_\infty\, c\, /\upsilon$, U_∞ is the free stream velocity, and c the chord length. LDV measurements for the mean velocity and a few turbulent quantities over the plate are available at Crompton´s study (2001), for attack angles α, varying from 1 to 5 degrees, in 1 degree intervals.

The same Reynolds number $Re = 2.13 \times 10^5$ and an inclination angle equal to 1^o was employed to compare the turbulence models results with Crompton´s experimental data.

Figure 3 shows the computational domain used in simulations, which was defined based on the work of Collie et al. (2008). At the inlet, the cartesian components of velocity are set according to the angle of attack and the free-stream turbulence intensity defined as $\varsigma = (1/3)(\overline{u'u'} + \overline{v'v'} + \overline{w'w'})/U_\infty^2 = (2/3)\,\kappa/U_\infty^2$ is set as 0.05%, as measured in the wind tunnel (Crompton, 2001). Constant pressure equal to the free stream p_∞ is set at the outlet.

Figure 2. Thin flat plate dimensions.

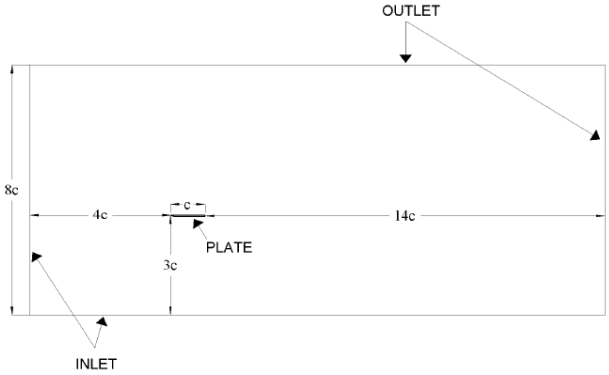

Figure 3. Domain details.

The plane mesh for RANS models was created in the software GAMBIT with 149 389 cells, a slightly larger number of points than employed by Collie et al. (2008), based on a grid convergence study performed by him. The maximum mesh expansion rate was kept below 1% in the region around the plate, while in the rest of the computational domain, away from the plate, a value of 5% was allowed. The distance of the first node above the plate was designed as 6.25×10^{-5} c to guarantee y^+ around 1, which is the value indicated for both SST κ–ω and LES.

To obtain the three-dimensional mesh for LES, the plane mesh for RANS was expanded in the spanwise direction (perpendicular to the plan of the Fig. 3), with length 0.25 c and divided in 16 parts generating a mesh with 2 390 324 control volumes, as recommended by Sampaio (2006), who investigated the correlation length in the spanwise direction. The boundary condition in the spanwise direction was set as periodic.

To flow field was determined with the commercial software Fluent with all models described in section 2. This code is based in Finite Volume Method. The interpolation scheme for RANS simulations was the QUICK scheme, while for LES, the Central-Differencing scheme was used. The pressure-velocity coupling was handled by the SIMPLE and PISO algorithms, respectively, for RANS models and LES simulations. The system of algebraic equation was solved with the Additive Multgrid method. The problem was considered converged when the maximum residue of all equations was smaller than 10^{-6}.

4.1. Reattachment length

Due to the abrupt geometry at the leading edge, separation of the boundary layer occurs and a long and thin bubble is created. Since the inclination angle is positive, the stagnation point is located below the surface of the plate and due to the high inertial forces (high Reynolds number) the particles do not follow the abrupt curvature of the extremity and separation occurs. The separated shear layer is unstable and transition rapidly occurs. After transition, a rapid development of the shear layer occurs due the high rate of turbulence entrainment, which bends the streamlines toward the surface of the plate at the reattachment point X_R. Now, due to the favorable pressure gradient existent between the larger pressure point in the reattachment point and the minimum pressure point close to the bubble center, the portion of the flow that goes back to the leading edge suffers a relaminarization process. The boundary layer of this portion of the flow moves forward to the leading edge becoming again laminar and ready to suffer a second separation, generating a secondary recirculation bubble, since there is another adverse pressure gradient at the minimum pressure point in the center of the bubble to the leading edge. This second very small bubble is very hard to be predicted, and it was only observed with LES Dynamic model.

Table 1 presents the reattachment lengths (X_R) for the flat plate at 1° incidence angle, obtained by the present work. The results obtained by Collie et al. (2008) with the κ–ω and SST κ–ω models employing the CFX software are also presented. Sampaio et al. (2006) investigated the same problem with the traditional one-equation model (Kim and Menon, 1997) and with the f-LES methodology (Sampaio, 2006), and obtained better results with the latter formulation, which is also present at Table 1.

The accuracy of the prediction of the reattachment lengths for this flow is strongly dependent on the ability of the turbulence model to represent the complex flow structure described; however the mesh refinement also plays a crucial part on this performance. It can be seen in Table 1, that the worse prediction was obtained with κ–ω model due to its deficiency in accurately predicting the free stream flow. Although the Spalart-Allmaras model predicted a better result than the κ–ω model, Rezende & Nieckele (2007) showed that this model is not able to predict the normal turbulent fluctuations. Since the SST κ–ω model blends the precise formulation of the κ–ω model close to walls with the free-stream independence of the κ–ε model outside the boundary layer, smaller errors in the X_r values were obtained. Note the improvement in the result reached here with the SST κ–ω model in relation to the one obtained with the same model by Collie et al. (2008), which shows the influence of a more refined mesh. Note also that, while the SST κ–ω models overestimated the X_R value, the model RSM underpredicted this value, but with a smaller error, since it is capable of representing the flow anisotropy which is fundamental to the accurate predictions of the thin bubble at the plate leading edge. Finally, it is evident in

Table 1 that the LES Dynamic model, with more refined mesh, provided the best result, not only because it can capture the large structures, but also the transfer of energy between scales and its dissipation at the small scales. The prediction of the f-LES methodology was equivalent to the RSM prediction, due to the relatively course mesh employed in that work. It is believed that with a more refined mesh the f-LES model will present more accurate results.

Table 1 – Normalized reattachment lengths (X_R) and respective errors.

	Experimental Crompton (2001)	LES Dynamic	SST κ–ω	RSM	SA Rezende & Nieckele (2007)	κ–ω Collie et al. (2008)	SST Collie et al. (2008)	f-LES Sampaio et al. (2006)
X_R / c	0.1400	0.1409	0.1456	0.1370	0.1520	0.1840	0.1490	0.1359
Error %		0.64	3.85	2.21	8.35	24.0	5.80	3.00

4.2. Mean velocities profiles

The mean velocities profiles obtained with SST κ–ω, RSM and LES Dynamic models are compared with the experimental data de Crompton (2001) at four stations. Figure 4 corresponds to the station x/c = 0.031 inside the bubble, where in Fig. 4b a zoom in the near wall region is shown. Figure 5 presents the velocity profiles for the remaining selected stations. Those stations are: x/c = 0.125, also located inside the bubble, while x/c = 0.250 and x/c = 0.375 stations are outside the bubble.

By examining Figs. 4 and 5, it can be seen that in general, the LES results showed an excellent agreement with the experimental data, especially when compared with the results of SST κ–ω and RSM simulations.

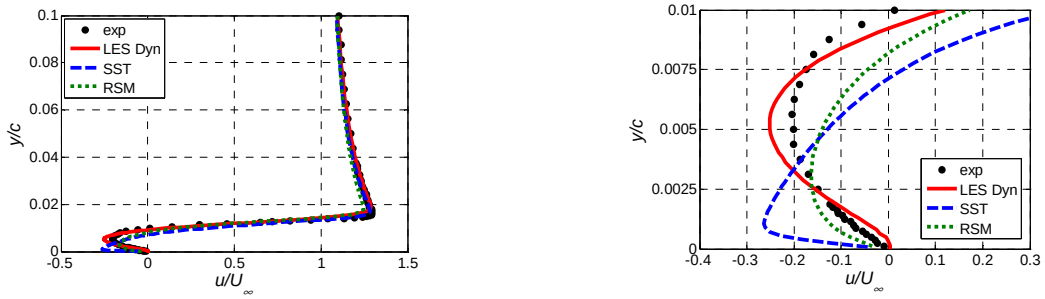

(a) x/c=0.031 (b) detail at x/c=0.031

Figure 4. Mean velocity profile inside the leading edge bubble.

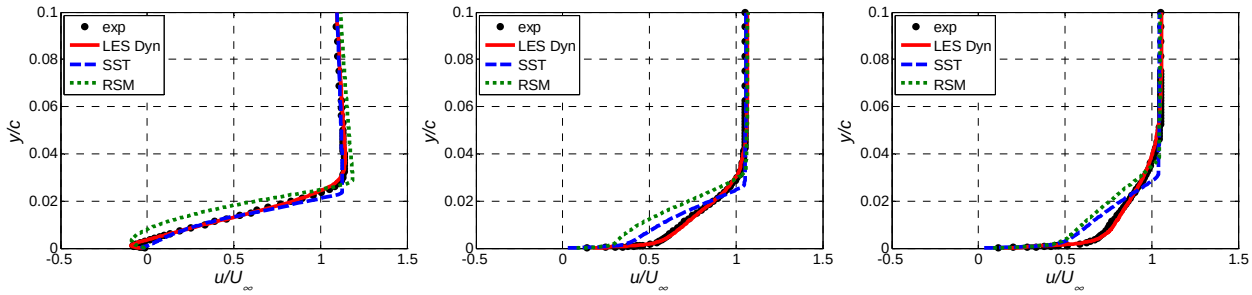

(a) x/c=0.125 (b) x/c=0.250 (c) x/c= 0.375

Figure 5. Mean velocities profiles at three stations.

The reversed flow inside the leading edge bubble experiences relaminarisation and the boundary layer begins to show very laminar features. Note in Fig. 4b (x/c = 0.031) that only the LES Dynamic model was able to predict this behavior, presenting a very good agreement with the experimental data. By examining Fig. 5, it can be seen that both RANS model showed a more smooth profile near the wall after the reattachment point, in the boundary layer developing region, indicating that the model is less diffusive. Note also, that although the X_r prediction of the RSM model was superior to the SST κ–ω prediction, the mean velocity profile presents the worst agreement with the experimental data.

Figure 6 shows the streamlines for the LES Dynamic, SST κ–ω and RSM models, close to the leading edge, in the region of the main recirculation bubble. It can be verified that only the LES model was able to predict the second recirculation bubble, which is observed experimentally. The absence of the secondary bubble in the RANS predictions

is directly related to the more turbulent velocities profiles foreseen by those simulations, inducing the flow inside the bubble to be more resistant to the second separation, keeping the reverse boundary layer attached to the plate inside the main bubble.

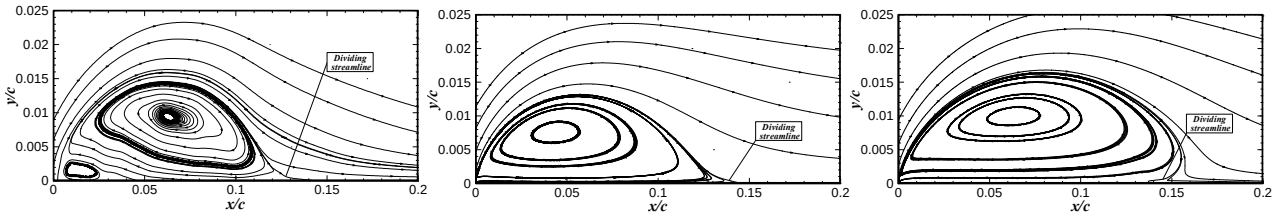

(a) LES Dynamic (b) SST κ–ω (c) RSM

Figure 6. Streamlines for the LES Dynamic, SST κ–ω and RSM models.

By examining Fig. 6c corresponding to the RSM model predictions, an anomalous behavior of the flow can be seen near the reattachment point. Note that the streamline, which divides the main flow from the bubble flow, bends back to reattachment point due to the existence of folds in the velocities profiles close the wall. This is a spurious result, which has already been observed by Hanjalic and Jakirlic (1998), when examined the backstep flow case with the RSM LRR model. This behavior is intensified, especially when refined meshes are employed, even when using the wall treatment mentioned in the section 2.2, as is the case of the present paper. In less refined meshes cases, the use of the logarithmic wall law masks this anomaly. There are several possible causes for this problem, including numerical error and wall law inadequacy; however Hanjalic and Jakirlic (1998) concluded that, without identifying the specific source of the spurious result, the model was inadequate to be used in the presence of boundary shear layer flows. Lasher and Taulbee (1992) attributed the cause of the problem to the coefficients for the pressure term Φ_{ij} of the LRR model and to the viscous dissipation model ε (section 2.2).

Aiming to identify the cause of the problem just described, the RSM model was also tested with two different treatments for the near wall region, without employing the LRR model for the pressure term. The first one is the RSM SSG model (Speziale et al., 1991) that adopts a quadratic model for the pressure term; and the second one is a model that blends RSM and κ–ω models near the wall (Wilcox, 1998). However, convergence was not attained with either model. This convergence difficulty is described explicitly in the Lasher and Sonnenmeier (2008) work, who were only able to obtain converged solution when adopted the first order Upwind interpolation scheme for the advective terms. Fadai-Ghotbi et al. (2008) also mentions this convergence problem in their transient simulations (URANS - Unsteady Reynolds Averaged Navier-Stokes). They also employed the first order Upwind interpolation scheme to obtain convergence, which introduced false diffusion, damping the fluctuations, and as a result the same profiles as the steady state RSM solution were obtained.

4.3. Pressure distributions

The pressure distribution can be analyzed through the pressure coefficient defined as

$$C_P = (p - p_\infty)/(0.5\,\rho\,U_\infty^2) \tag{9}$$

where p is the static pressure, p_∞ and U_∞ are the freestream pressure and velocity.

Figure 7a presents the pressure contour near the leading edge. The stagnation point in the lower side of the plate can be clearly seen. A visible suction can also be seen inside the bubble region, in the upper side of the plate, by the significant pressure reduction. After the reattachments point, the pressure is approximately constant. Figure 7b illustrates the pressure coefficient along the plate. Again the SST κ–ω, RSM and LES Dynamic models are compared with the experimental data. Excellent prediction was obtained with the LES Dynamic model, which reproduced the experimental data, because it was able to capture the second recirculation bubble. Smaller suction was predicted by both RANS models. The lack of the second bubble prediction leads the SST κ–ω model to anticipate the pressure recovery. The anomalous flow behavior at the reattachment region, seen with the RSM model, reflected on the pressure distribution, resulting in a smaller peak and smoother drop.

4.4. Turbulent quantities

The turbulent axial second order statistics $\overline{u'u'}$ predicted with SST κ–ω, RSM and LES Dynamic models are compared with the experimental data in Fig. 8 for incidence angle $\alpha = 1^0$.

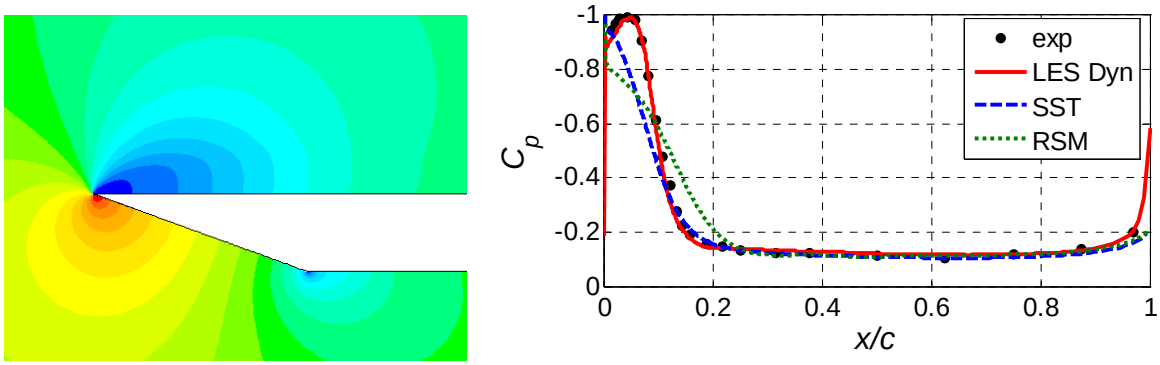

(a) Isolines of constant pressure at the leading edge (b) Pressure coefficient distribution along plate

Figure 7. Pressure distribution.

Analyzing the graphs in Fig. 8, it can be seen that turbulence is generated in the recirculating zone, inside the leading edge bubble. As one moves along the plate, the turbulence intensity decreases, but the region affected by turbulence gets wider. Once again the agreement of the LES Dynamic model results with the experimental data is very good, not only inside the bubble but also after the reattachment point. The RSM model was able to predict the same level of turbulence intensity, but it underestimates $\overline{u'u'}$ near the reattachment point (Fig. 8b) and overestimated it after, at stations x/c = 0.250 and 0.375 (Figs. 8c and d). In spite of the spurious results near the reattachment point, reasonable results were obtained with RSM since $\overline{u'u'}$ is determined from its transport equation, i.e., it involves less modeling than the SST κ–ω model.

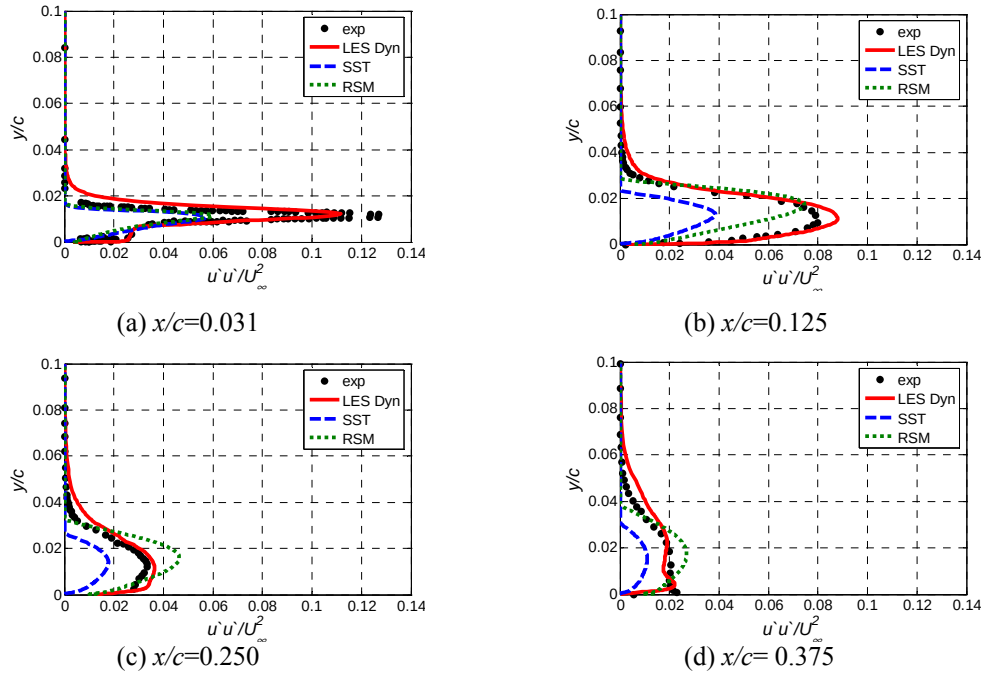

(a) x/c=0.031 (b) x/c=0.125

(c) x/c=0.250 (d) x/c= 0.375

Figure 8. Axial second order statistics $\overline{u'u'}$.

The SST κ–ω model calculates $\overline{u'u'}$ through Eq. (3), with the turbulence viscosity obtained by blending the standard κ–ω in the near-wall region with the standard κ–ε model across the outer region. Figure 9 illustrates the viscosity ratio υ_t/υ, for the SST κ–ω model along the plate, showing the peak of turbulent viscosity at the bubble region center ($x/c \approx 0.05$, as shown in Fig. 6b). Figure 8 shows that the turbulent axial second statistic is underestimated by SST κ–ω model in all section analyzed, which explains the smoother mean velocity gradient observed in Fig. 5.

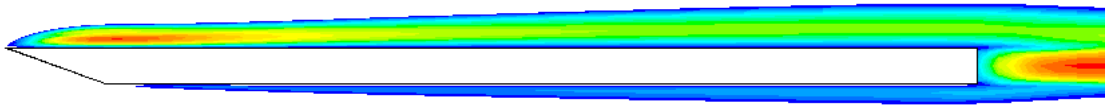

Figure 9. Contour of viscosity ratio υ_t/υ, for the SST model.

Figure 10 illustrates the turbulent kinetic energy distribution near the leading edge, for the SST κ–ω model, where it can be clearly seen that the generation of turbulence occurs very close to the edge and it has a direct connection with the strong pressure drop reduction. The result shown in Fig. 10 also complements the information obtained by the $\overline{u'u'}$ profiles presented in Fig. 8, showing that the main contribution to the kinetic energy is due to the axial second order statistics.

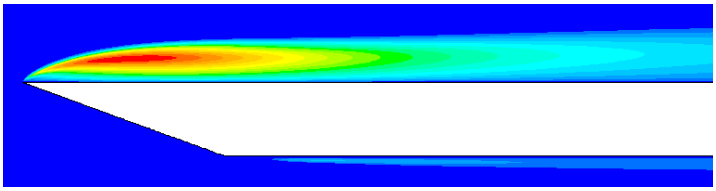

Figure 10. Contour of turbulent kinetic energy. SST κ–ω model.

An interesting parameter which can give information about the coherent structures is the Q-criteria, which can be defined as

$$Q = \frac{1}{2}\left[\overline{\Omega_{ij}}\;\overline{\Omega_{ij}} - 2\,\overline{S_{ij}}\;\overline{S_{ij}}\right] \qquad \text{where} \qquad \overline{S_{ij}} = \frac{1}{2}\left(\frac{\partial \overline{u_i}}{\partial x_j} + \frac{\partial \overline{u_j}}{\partial x_i}\right) \quad \text{and} \quad \overline{\Omega_{ij}} = \frac{1}{2}\left(\frac{\partial \overline{u_i}}{\partial x_j} - \frac{\partial \overline{u_j}}{\partial x_i}\right) \tag{10}$$

Figure 11 illustrates the contours of the Q-criteria for the SST κ–ω model. Note the high values near the leading edge, indicating the formation of coherent vortices, which quickly disappear, since the model is steady state and 2D.

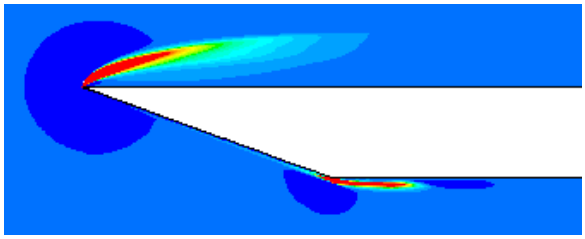

Figure 11. Contour of the Q criteria at the leading edge. SST κ–ω model.

5. CONCLUSION

In the present work, the turbulence models RSM (Launder, 1989), SST κ–ω (Menter, 1994) and LES Dynamic (Germano et al., 1991; Lilly, 1992) were applied to determine the incompressible flow over a flat plate with a sharp leading edge, with an inclination angles $\alpha = 1^0$. The results obtained were compared with experimental data of Crompton (2001).

The RANS models predicted mean velocities profiles which presented reasonable agreement with the experimental results; however none of the RANS models captured the second recirculation bubble and a correct entrainment in the boundary shear layer, causing deviations in the velocity and pressure field in the bubble region.

Due the inability to calculate the flow in the recirculation zone, the SST κ–ω model presents poor pressure prediction quality close to the leading edge, anticipating the pressure recovery. The RSM model produced a velocity field with an anomaly, which influenced the pressure coefficient distribution, reducing its peak and smoothing the pressure recovery.

In general, the SST κ–ω model can be considered superior to the RSM model, since it requires less simulation time, and the results were more coherent. The RSM model showed good results for $\overline{u'u'}$, but it presented difficulty of convergence, high computational cost and spurious velocity at the reattachment region.

The results obtained with the LES Dynamic model were better than those predicted by the RANS models. The leading edge bubble was accurately predicted, presenting excellent agreement for the reattachment length. The LES Dynamic model was able to predict the second recirculation bubble, and as a consequence the obtained velocity and pressure fields were in good agreement with the experimental data.

6. ACKNOWLEDGEMENTS

The authors acknowledge the support awarded to this research by the Brazilian Research Council, CNPq.

7. REFERENCES

Cazalbou, J.B., Spalart, P.R., Bradshaw, P., 1993, "On the Behavior of 2-Equation Models at the Edge of a Turbulent Region", Physics of Fluids, Vol. 6, No. 5, pp. 1797-1804.

Chen, H.C. and Patel V. C., 1988, "Near-Wall Turbulence Models for Complex Flows Including Separation". AIAA Journal, Vol. 26, No. 6, pp. 641-648.

Collie S., Gerritsen M., Jackson P., 2008, "Performance of Two-Equation Turbulence Models for Flat Plate Flows with Leading Edge Bubbles". Journal of Fluids Engineering-Transactions of the Asme, Vol. 130, No. 2.

Crompton, M., 2001, "The Thin Airfoil Leading Edge Separation Bubble", PhD Thesis, Department of Aerospace Engineering University of Bristol.

Durbin, P.A., 1995, "Separated Flow Computations with κ - ε - v^2 Model". AIAA Journal, Vol. 33, No. 4, pp. 659-664.

Fadai-Ghotbi, A., Manceau, R. and Boree, J. , 2008, "Revisiting URANS Computations of the Backward-Facing Step Flow Using Second Moment Closures. Influence of the Numerics". Flow Turbulence and Combustion, Vol. 81, No. 3, pp. 395-414.

Germano, M., Piomelli, U., Moin, P., Cabot, W. H., 1991, "A Dynamic Subgrid-Scale Eddy Viscosity Model". Phys. Fluids A, Vol. 3, No. 7, pp. 1760-1765.

Gibson, M.M. and Launder B.E., 1978, "Ground Effects on Pressure-Fluctuations in Atmospheric Boundary-Layer" Journal of Fluid Mechanics, Vol. 86, pp. 491-511.

Hanjalic, K. , 1994, "Advanced Turbulent Closure Models: a View of Current Status and Future Prospects". International Journal of Heat and Fluid Flow, Vol. 15, pp.178-203.

Hanjalic, K., Jakirlic, S. , 1998, "Contribution Towards the Second-Moment Closure Modeling of Separating Turbulent Flows". Computers & Fluids, Vol. 27, No. 2, pp. 137-156.

Kim, W.W. and Menon S., 1997, "Application of the Localized Dynamic Subgrid-Scale Model to Turbulent Wall-Bounded Flows". AIAA, 35^0 Aerospace Sciences Meeting, Reno, Nevada.

Launder, B. E., Reece, G. J. and Rodi W., 1975, "Progress in the Development of a Reynolds-Stress Turbulence Closure". Journal of Fluid Mechanics, Vol. 68, No. 3, pp. 537-566.

Launder B. E., 1989, "Second-Moment Closure: Present... and Future?" , International Journal of Heat and Fluid Flow, Vol. 10, No. 4, pp. 282-300.

Lasher, W.C. and Taulbee, D.B. , 1992, "On the Computation of Turbulent Backstep Flow". International Journal of Heat and Fluid Flow. Vol. 13, No. 1, pp. 30-40.

Lasher, W.C. and Sonnenmeier, J.R. , 2008, "An Analysis of Practical RANS Simulations for Spinnaker Aerodynamics". Journal of Wind Engineering and Industrial Aerodynamics. Vol. 96, pp. 143-165.

Lien, F.S., Leschziner, M.A., 1994, "Assessment of Turbulent Transport Models Including Non-Linear RNG Eddy-Viscosity Formulation and Second-Moment Closure". Computers and Fluids, Vol. 23, No. 8, pp. 983-1004.

Lilly, D. K., 1992, "A Proposed Modification of the Germano Subgrid-Scale Closure Method". Physics of Fluids A, Vol. 4, No. 3, pp. 633-635.

Menter, F. R., 1994, "Two-Equation Eddy-Viscosity Turbulence Models for Engineering Applications", AIAA Jounal, Vol. 32, No. 8, pp. 1598-1605.

Newman, B. G. and Tse, M. C., 1992, "Incompressible-Flow Past A Flat-Plate Aerofoil With Leading-Edge Separation Bubble", Aeronautical Journal, Vol. 96, No. 952, pp. 57-64.

Rezende, A.L.T. and Nieckele, A.O., 2007, "Prediction of the Flow Over a Thin Flat Plate at Shallow Incidence", Proceedings of the 19th International Congress of Mechanical Engineering – COBEM 2007.

Rezende, A.L.T. Sampaio, L.E.B and Nieckele, A.O., 2008, "Reynolds Average Navier-Stokes Simulation of Highly Anisotropic Turbulence Structures", Proceedings of the 6th Spring School of Transition and Turbulence, EPTT 2008.

Sampaio, L. E. B. ; Nieckele, A. O. ; Gerritsen, M. ; Collie, S., 2006, " Numerical Simulations Of The Long Recirculation Bubbles Formed In Incompressible Aerodynamic Flows Over Thin Flat Plates At Shallow Incidence.", Proceedings of 11th Brazilian Congress of Thermal Sciences and Engineering, ENCIT 2006.

Sampaio, L. E. B, "Simulação de Grandes Escalas da Bolha de Separação em Placas Finas em Pequeno Ângulo". Tese de Doutorado - Departamento de Engenharia Mecânica, PUC, Rio de Janeiro, 2006..

Spalart, P. and Allmaras, S., 1992, "A one-equation turbulence model for aerodynamic flows", Technical Report AIAA-92-0439, American Institute of Aeronautics and Astronautics.

Speziale, C. G., Sarkar S. and Gatski, T. B. , 1991, "Modelling the Pressure-Strain Correlation of Turbulence: an Invariant Dynamical Systems Approach". Journal of Fluid Mechanics, Vol. 227, pp. 245-272.

Wilcox, D.C., 1998, "Turbulence Modeling for CFD". Ed. DCW, Califórnia, EUA.

Wolfshtein, M., 1969, "The Velocity and Temperature Distribution of One-Dimensional Flow with Turbulence Augmentation and Pressure Gradient", International Journal of Heat and Mass Transfer, Vol. 12, pp. 301-318.

8. RESPONSIBILITY NOTICE

The authors are the only responsible for the printed material included in this paper.